

# **STGIC: a graph and image convolution-based method for spatial transcriptomic clustering**

Chen Zhang<sup>a#</sup>, Junhui Gao<sup>a#</sup>, Guangshuo Cao<sup>b</sup>, Wei Liu<sup>c</sup>

<sup>a</sup>AI Research Center at Shanghai Nuanhe Brain Technology Co. Ltd., Shanghai, 200030, China

<sup>b</sup>State Key Laboratory of Public Big Data, College of Computer Science and Technology, Guizhou University, Guiyang

<sup>c</sup>Hangzhou Huoshi Digital Intelligence Technology Co., Ltd

\*To whom correspondence should be addressed: Chen Zhang, Email: zhang83890@sina.com

#These authors contributed equally to this work.

## **Abstract**

Spatial transcriptomic (ST) clustering requires dividing spots into spatial domains, each of which are constituted by continuously distributed spots sharing similar gene transcription profile. Adjacency and feature matrix being derived respectively from 2D spatial coordinates and gene transcription quantity, the problem is amenable to graph network. The existing graph network methods often employ self-supervision or contrastive learning to construct training objectives, which as such are not directly related to smoothing embedding of spots and thus hard to perform well. Herein, we propose a graph and image-based method (STGIC) which adopts AGC, an existing graph-based method not depending on any trainable parameters for generating pseudo-labels for clustering by our dilated convolution network (CNN)-based frameworks which are fed with virtual image also transformed from spatial and transcription information of spots. The pre-defined graph convolution kernel in AGC plays a key role as a low-pass filter in smoothing, which can be further guaranteed by our training loss demanding embedding similarity between neighboring pixels. Our dilated CNN-based frameworks are featured by two parallel components respectively with convolution kernel size of 3 and 2, besides some constraints are made on the convolution kernel weights. These fancied designs ensure spots information updates by aggregating only that from neighboring spots with the weights depending on the distance from kernel center. Apart from the above tricks, self-supervision and contrastive learning are also adopted in STGIC to construct our training objective. Tests with the generally recognized dataset DLPFC demonstrates STGIC outperforms the state-of-the-art methods.

**Keywords:** spatial transcriptomic clustering; graph convolution; dilated convolution; self-supervision; contrastive learning

## 1. Introduction

Single-cell transcriptomics (SC) technique has been fully developed to push forward greatly the research of life science at the level of transcriptomics via its advantage of a high resolution to make clear the transcriptomic profile in every single cell, thus its sequencing unit. SC clustering requires grouping cells of the same type together with gene transcription information. Methods originally for community detection have been used for SC clustering, such as Leiden and Louvain[1]. ST technique has also been rapidly developed in recent years. Compared with SC, it takes account of one more aspect of the spatial information of the sequencing unit, which is termed as a spot usually containing more than one cells. Resolution of existing ST technique is generally not so high as SC and the improvement of the resolution usually achieves at the cost of drop in the number of genes detected in one spot. At present, the ST platform of 10X Visium manages to reach a relatively ideal trade-off between the two conflicting aspects, gaining widespread recognition. ST clustering aims to divide all spots from a sample slice into spatial domains according to both spatial vicinity and gene transcription similarity. Each spatial domain consists of continuously distributed spots, all of which present relative coherence in transcription profile. Compared with SC clustering, ST clustering owns one more aspect of the cue from spatial information to help smooth spots features so that embedding similarity of spatially neighboring spots is enhanced and thus improve the clustering performance. Based on division of spatial domains, many significant downstream works can be done such as searching for spatial domain specific marker genes and spot-interaction prediction which are tremendously helpful to unearth the underlying biological mechanisms behind tissue development, onset and progression of disease [2].

The lag of related algorithm behind the improvement of hardware in ST field is quite conspicuous, which may be imputed to the poor availability of training data with authoritative ground-truth labels. The experimental labeling process is terribly time-consuming and costly. Although clustering as an unsupervised task needs no labels for training, Labels of high confidence remain necessary for performance test. Presently, the generally acceptable dataset for ST clustering is DLPFC which owns 12 slices of human dorsolateral prefrontal cortex with relatively high quality of labels assigned to nearly all spots of each slice [3]. So far, all ST clustering algorithms have been trained and tested with the 12 samples. The aforementioned algorithms Leiden and Louvain considering only gene transcription information had still been used for ST clustering until the naissance of the deep learning method SpaGCN in late 2021 which adopts graph convolution network (GCN) with an adjacency constructed from spatial coordinates and input of gene transcription information [4]. STAGATE is the second popular deep learning ST toolkit which carries out spots clustering by making use of graph attention network

(GAT) and auto-encoder framework to reconstruct the gene expression information, the spatial coordinates is used to identify neighborhood for each spot and gene transcription information is also inputted as feature matrix [5]. The clustering performance of STAGATE is significantly better than SpaGCN.

Besides deep learning, statistical methods have also been experimented with in ST clustering. The first statistical method is BayesSpace [6], but have an apparently poorer performance than STAGATE. SpatialPCA is another paradigm of statistical method for ST clustering and performs better than STAGATE [7], but the performance is still open to improve.

Graph deep learning and statistics have become the main media for ST clustering model. Insofar as the graph deep learning framework, the usage of vanilla graph convolution [8] is the highest for its containing fewer trainable parameters and causing no significant drop in performance compared with other form of trainable parameter containing graph convolution to treat the same graph. Nonetheless, the smoothing effect of the vanilla also depends on label supervision, which is absent from unsupervised training. Therefore, in our unsupervised task of ST clustering, we divert to a kind of graph convolution AGC with predefined kernel function and hence obviating trainable parameters to realize embedding smoothing. Another vantage of AGC lies in its underlying mechanism to prevent over-smoothing.

Comprehensively evaluating performances of existing graph deep learning method among the above 12 publicly recognized samples, we found that they consistently have a depressingly poor performance on the samples 151669 and 151670, suggesting there's some inherent limitations of the graph learning methods for the data characteristics of the two samples. To improve the general performance among the 12 samples, we have to improve the performance on the two samples significantly and simultaneously maintain good performance on the other samples. Therefore, in addition to AGC, other method not based on graph learning is incorporated into our algorithm to redeem the innate deficiency of graph-based method for the two samples. In light of the convertibility of graph derived from ST data to image as well as the similarity between the purpose of spots clustering and that of unsupervised image segmentation, the convolution neural network (CNN) based framework reported in a one-image-unsupervised-segmentation algorithm [9] is adopted and abbreviated as UISDC by us. The arrangement of spots at their 2D coordinates can form a regular lattice which can be deemed as an image. Within the image, spots can be treated like pixels and gene transcription information of spots can be transformed into pixel values. After the conversion, spots clustering into spatial domains can be interpreted as pixels clustering, which is rightly what unsupervised image segmentation tries to do. To make the image segmentation method really work for our task, some adaptations are made on the CNN framework of UISDC according to the

characteristic of spots spatial distribution of 10X Visium. Besides, several self-supervision and contrastive learning skills originally used in graph learning are also adapted to our CNN output feature image for constructing training objectives.

Through the above combination of graph and image methods and adaptation of graph skills to output image, we establish our own ST clustering method STGIC and manage to improve the performances on the sample 151669 and 151670 by a large extent and simultaneously keep high performance on other samples, thus boosting the general performance among all the 12 samples. Our contributions can be summarized as follows:

- We propose a CNN based framework specific to the ST sequencing platform 10x Visium.
- We provide a paradigm of the combination of graph convolution and image convolution for ST clustering, in which not only is the information gathering mechanisms is combined, but also skills to construct training objectives in graph learning is grafted to treat image output. To our knowledge it is the first time that graph method and image method have been unified to solve ST clustering problem.

## **2. Related works**

Since the advent of graph convolution, its various variants have been emerging to solve node-level tasks such as node classification, link prediction and node clustering, together with graph-level tasks such as graph classification. An attributed graph contains two essentials which are adjacency to describe the correlation between nodes and feature matrix to describe the feature of each spot. Community detection problem often includes the two aspects of information and requires data points to be divided into clusters, hence always treated with graph convolution method as node clustering task which often resorts to skills of self-supervision and contrastive learning to construct training objectives.

DGI [10] and GIC [11] exemplify contrastive learning skills in community detection by extracting information through graph convolution from multiple views and constructing objective functions for training via the estimation of mutual information (MI). Node embedding computed from original graph is often considered as information in view 1. Permutation of rows or randomly masking some columns in feature matrix generates a perturbed feature, from which information can be derived in view 2. The contrastive learning is achieved by comparison between the two views. In DGI, graph summary is computed from view 1 and mutual information between embedding and graph summary in view 1 is expected to be large since they are both from the same view, however, that between embedding in view 2 and graph summary is expected to be small since they are from different views. Apart from graph summary, GIC also computes cluster summary from view 1 with which to substitute graph summary to compute MIs between the two

views. Besides perturbation on feature matrix, modification can also be made on adjacency to form multiple views, such as DCRN [12] which randomly change some elements in adjacency to be 0, meaning deletion of some connections between nodes and change some 0 elements to be non-zero according to pre-training embedding, meaning adding some edges to graph.

In contrast to all the above methods depending on neural network with trainable parameters. AGC pre-defines a Fourier transformed graph convolution kernel function to ensure low-pass filtering perform smoothness of node embeddings without dependence on any trainable parameter [13]. Moreover, its proposal of the condition for iteration termination according to the intra-cluster distance effectively avoiding over-smoothing.

Conversion of ST data into a graph with adjacency and feature matrix is quite common to deal with ST clustering in which spots spatial information in ST data is used to compute an adjacency and gene transcription information is pre-processed to generate an input feature matrix. SpaGCN is the first to solve ST clustering with GCN with the help of a self-supervision skill. The only one GCN layer used by SpaGCN adopts the simplest vanilla form which was deduced with self-looped adjacency, supposing the largest eigen-value of normalized Laplacian matrix to be 2, approximating Fourier transformed graph convolution kernel function with two-order Chebyshev polynomial and setting the two corresponding trainable parameter matrices to be mutually inverse. In SpaGCN, an additional dimension of coordinates extracted from H&E staining image is incorporated into the 2D spatial coordinates to generate a 3D coordinates from which a distance matrix is computed and further an adjacency is derived according to the distance matrix via a Gaussian kernel function. The top 50 Principal Components (PCs) of normalized expression matrix is taken as the input of the graph convolution. Finally, the training is performed with the objective of a Kullback-Leibler (KL) divergence with the target distribution derived from cluster assignment probability distribution directly, which is considered to be a self-supervision skill for the target distribution is also deduced from the other in the divergence.

STAGATE is another method to use graph learning to solve ST clustering. Instead of GCN, it employs several layers of graph attention network (GAT) arranged in an auto-encoder structure, with the trainable parameter matrix of corresponding layer of the encoder and the decoder to be transpose of each other. The loss function adopted is the mean square error (MSE) between the preprocessed gene transcription matrix and its reconstruction. STAGATE have a significantly higher performance than SpaGCN when testing with the dataset DLPFC.

In contrast with the readiness of ST data being transformed to an attributed graph, its conversion to image is much more indirect and complex. Once arranged at the spatial coordinates, spots are distributed regularly in a lattice which can be treated like an image

with each spot taken as a pixel and with pixel values transformed from gene transcription information.

Such a reasonable transformation of ST data to image enables clustering with methods originally designed for unsupervised image segmentation. However, unsupervised image segmentation is often treated with complex neural network and the training depends in most cases on trainable parameters initiated with pretraining-derived values, and the pre-training is often performed on a supervision basis with large quantities of ground-truth labeled images. In addition, both pre-training and training demand more than one image input as a batch. These requirements are difficult to meet in ST clustering, since there are not enough samples with ground-truth labels for supervised pre-training so that the algorithms thereof are always tested only on the above 12 samples and the high heterogeneity between biological samples demand values of trainable parameters to be sample-specific and hence the training is often performed with one single sample in each iteration. However, UISDC emerges as an exception among one-image-unsupervised-segmentation methods. It doesn't need the trainable parameters to be initiated by pretraining-derived values and is fed with only one image in an iteration. These advantages of UISDC suggests the underlying feasibility in our task. On the other hand, we also find the convolution in UISDC have some characteristic in common with graph convolution. All convolution layers in UISDC consistently adopt the kernel size of 3, making sure that all pixels update features by aggregating the information from only the 8 surrounding neighbors along with themselves. The selected neighbors are the nearest to each pixel in all directions for an image, much like the direct neighbor of any node in a graph. Therefore, the information-gathering manner of UISDC is similar to the information-aggregation from only the direct neighbor in a graph by GCN with binary adjacency whose elements at the diagonal and corresponding to connections with direct neighbors are 1 and otherwise 0. The use of padding in the convolutions enables the unchanged size from the input to the output, which guarantees all pixel remains after each convolution operation as all nodes persist after each graph convolution filtering. The similarity between graph convolution and the CNN in UISDC lends justification to our method STGIC which generates spots embedding from image output by CNN and treats the CNN-derived embedding with loss functions originally designed for graph learning.

In the following, we will elucidate how STGIC works to solve ST clustering in terms of the mathematical principles, the pre-processing of ST data, application of AGC in the pre-training stage, adaptation of the CNN in UISDC to form our own frameworks and training skills for our network.

### **3. Proposed work**

#### **Problem Definition**

ST data is often stored as AnnData structure in h5ad file which can be read by a

python package scanpy [14]. The main information in h5ad file including pixel coordinates, lattice coordinates, gene names and gene expression matrix with each row corresponding to each spot and each column to each gene. By pixel coordinates of a spot, we mean the 2D coordinates of a pixel in the H&E staining slice the spot corresponds to. Because of the technical limitation, only a few pixels in the slice have corresponding spots. If marking all the spots-corresponding pixels in the staining slice, we can easily find these spots distributed quite regularly so that they can be contained in a rectangular lattice which is filled with additional points at the midpoint of the line between any pair of neighboring spots and at peripheral area surrounding all the spots. The lattice can be treated as an image and its points as pixels. The virtual image transformed from the lattice is denoted as  $X_{img}$ . In  $X_{img}$ , each pair of the nearest neighboring spots is partitioned by one pixel corresponding to none of spots and surrounding the spots area are also pixels without any corresponding spots. The pixels with corresponding spots are termed spot pixels, the pixels partitioning neighboring spots are termed null pixels and the peripheral pixels surrounding spots area are termed background pixels. A small part of the lattice and the partition of neighboring spots by null pixels are illustrated in Fig. 1. The position of all pixels in  $X_{img}$  can also be indicated with 2D coordinates, which is referred to as lattice coordinates herein to differentiate from pixel coordinates in staining image. ST clustering takes spatial information and gene transcription information of spots to assign each spot to a cluster label. In our STGIC, a graph is constructed with each node corresponding to each spot, the adjacency is computed from spatial distances between spots and the transcription profile can be transformed into feature of each spot. Such an attributed graph can be treated with graph convolution. besides,  $X_{img}$  is taken as input for CNN. With the combination of graph convolution and CNN, STGIC completes the cluster label assignment.

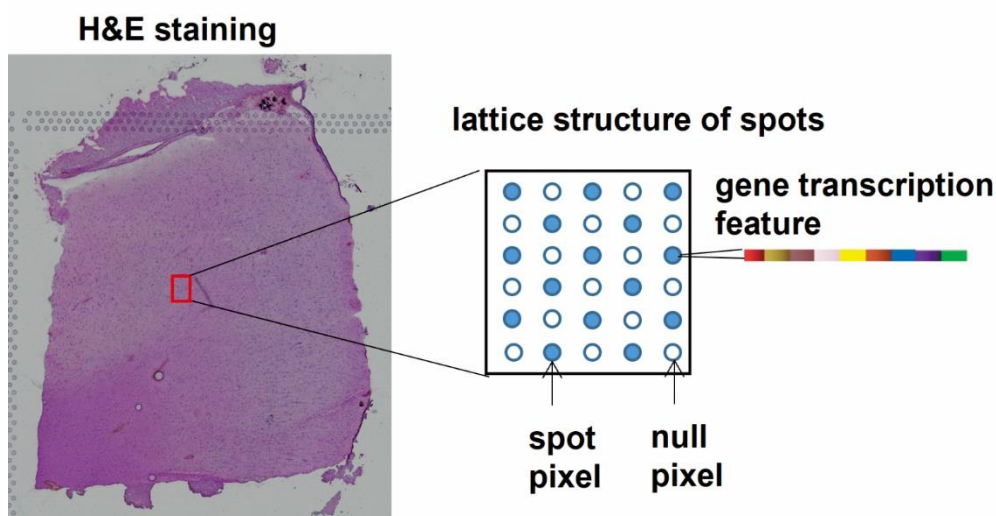


Fig. 1. Transformation of ST data into a virtual image. Solid circle represents spot pixel while hollow circle represents null pixel. Null pixel doesn't really exist in the lattice. Showing it in the lattice facilitates

interpreting the lattice as an image and makes clear the separation of neighboring spots by one null pixel in the virtual image. Gene transcription information is presented with a colorful bar consisting of color blocks, each of which corresponds to the transcription quantity of a detected gene.

### 3.1. Graph convolution neural network

Convolution is in itself a kind of wave filter with no exception of its application to graph. usually the signal of high frequency contains noises while that of low frequency tends to be composed of more useful information, hence an ideal convolution is expected to preserve more low-band signal while filtering out high-band. Before elucidating the graph convolution adopted herein, the mathematical principle of graph convolution is introduced. Fourier and the inverse transformation play important role in calculating convolution in the data of graph, as do they in the problem of convolution computation in non-graph data. To get the basis for Fourier and its inverse transformation, the following operations are performed. For a graph with  $n$  nodes, the adjacency matrix  $A$  and the degree matrix  $D$  can be used to compute the Laplacian matrix  $L=D-A$ , which is then symmetrically normalized by  $D^{-1/2}$  to get  $L_s = I - D^{-1/2}AD^{-1/2}$ . The normalized Laplacian matrix can be eigen-decomposed in the form of  $U\Lambda U^{-1}$ ,  $\Lambda$  is the diagonal matrix with the eigen-values  $\lambda_1 \geq \lambda_2 \geq \dots \geq \lambda_q \geq \dots \geq \lambda_n$  at the diagonal, among which  $\lambda_1$  is the largest eigen-value and hence also denoted as  $\lambda_{max}$ . These eigen-values are the frequencies of the graph,  $U$  is the corresponding eigen-matrix (sometimes  $U^{-1}$  is substituted with  $U^T$  as the inverse of  $U$  equals its transpose for real symmetric matrix  $L_s$ ). All columns of  $U^{-1}$  constitute a group of basis for graph Fourier transformation while those of  $U$  for the inverse transformation. Every column of the feature matrix  $X$  provides a graph signal in the spatial field with the information of all nodes. Fourier transformation of  $f$  is realized by left multiplication of it with  $U^{-1}$ , likewise the same operation can be done to graph convolution filter, but in most cases, the convolution filter is not predefined and contains trainable parameters. Fourier transformation of a graph convolution kernel can be abstractly denoted as a column vector  $(g(\lambda_1), g(\lambda_2), \dots, g(\lambda_q), \dots, g(\lambda_n))^T$ , that is, the vector function of graph frequencies. According to Convolution Theorem that Fourier transformation of convolution between two functions amounts to the product of Fourier transformation of the two functions and the lemma that the inverse process of a Fourier transformation of a function return to the function itself, the filtered signal  $f'$  by the graph convolution filter can be simply denoted as  $Ug(\Lambda)U^{-1}f$  and further the compact form  $g(L_s)f$ . To construct GCN, Chebyshev polynomial which demands the independent variable fall into the range of the interval  $[-1,1]$  is often resorted to to approximate  $g(L_s)$ . The restriction on the range of the independent variable is obeyed by transformation of  $\Lambda$  to  $2\Lambda/\lambda_{max} - I$  and then  $g(L_s)$  can be approximated as

$$\sum_{k=0}^{K-1} w_k T_k(2L_s / \lambda_{max} - I),$$

$K$  is the order of Chebyshev polynomial, while  $w_k$  is Chebyshev polynomial coefficient corresponding to the order  $k$ .  $T_0(X)=I$ ,  $T_1(X)=X$ , and the recursion



formula is  $T_k(X) = 2XT_{k-1}(X) - T_{k-2}(X)$  (1)

All too often, the function  $g$  is not pre-defined, which makes the direct calculation of the polynomial coefficients impossible. The trouble is usually solved by constructing a neural network and fixing the coefficients on an iterative basis, and therefore the neural network is referred to as graph convolution neural network. If we set

$$L' = 2L_s / \lambda_{\max} - I \quad (2)$$

the  $j^{\text{th}}$  column of output matrix of a GCN can be computed with the formula:

$$f'_j = \sum_{k=0}^{K-1} T_k(L') \sum_{i=1}^{D_{in}} w_{kij} f_i \quad (3)$$

$D_{in}$  is input dimension,  $f_i$  is the  $i^{\text{th}}$  column of input matrix  $X$  and  $w_{kij}$  is an element of three-dimensional array of trainable parameters. In terms of matrix calculation, the output

of GCN can be computed in the formula:  $F_{out} = \sum_{k=0}^{K-1} T_k(L') F_{in} W_k$  (4)

$F_{in}$  is the input feature matrix, and  $W_k$  is the trainable parameter matrix corresponding to the  $k^{\text{th}}$  order of Chebyshev polynomial.  $F_{in} W_k$  in the formula acts to linearly transform the input feature,  $T_k(L')$  contains the information about the correlation between any pair of nodes determining the weights by which to aggregate the linearly transformed features when updating the feature of each node. The ultimate output of GCN is the sum of the aggregation output with  $T_k(L')$  of all orders.

### 3.2. Graph convolution with predefined kernel

GCN works well in supervised semi-supervised learning since ground truth is available for training to force the trainable parameters of the convolution filter to be adjusted well enough to extract information within an appropriate waveband. However, in our clustering task, the ground truth is absent from training, the adjusting of filter parameters becomes much more difficult even though contrastive and self-supervising tricks can alleviate this plight to some extent. To circumvent the obstacle impacting the efficiency of wave filtering in graph, a predefined convolution filter function was designed in the algorithm AGC which manages to appropriately smooth embedding among neighboring nodes. Laplacian-Beltrami operator establish the negative correlation between graph frequency  $\lambda_q$  and the smoothness of its corresponding Fourier basis  $u_q$  suggesting the signal containing higher proportion of low frequency components is smoother [13]. Signal  $f$  can be decomposed by inverse Fourier transformation into  $UZ$ ,  $Z$  is a column vector comprising the coefficients corresponding to the basis of the inverse transformation. Substituting  $f$  with the decomposed form leads to the following formula to

compute the filtered signal  $f'$ :  $f' = \sum_{q=1}^n g(\lambda_q) z_q u_q$  (5)

$z_q$  is the weight of the basis  $u_q$  and the  $q^{\text{th}}$  element of  $Z$ .  $g(\lambda_q) z_q$  is the coefficient of the

basis  $u_q$ . Decreasing the coefficient of high frequency corresponding basis drops the proportion of high frequency components and thus generates a smoother filtered signal  $f'$ . According to the corollary, adopting a decreasing and non-negative function in the interval  $[0, \lambda_{max}]$  for  $g$  meets the need of ideal smoothness. AGC adopt the following form of the function  $g$ :

$$g(\lambda_q) = 1 - \lambda_q / \lambda_{max} \quad (6) [13]$$

and  $f'$  can be calculated with the formula:  $f' = (I - L_s / \lambda_{max})f$  (7)

After several times of operation with the predefined Fourier transformed convolution kernel, the resulting filtered signal  $f'$  is smoothed, the output embedding from the initial feature input  $X$  through  $t$  times of the above smoothing operation is computed in the

$$Emb = (I - L_s / \lambda_{max})^t X \quad (8)$$

The value of  $t$  is also significant for the performance of the algorithm since  $t$  with less values may lead to insufficient smoothness while  $t$  with larger ones may cause over-smoothness. As proposed in AGC, the intra-cluster distance of node embedding is suitable for determining when to stop the smoothing operation. Smoothing can enhance the similarity among neighboring nodes, which would mainly cause decrease in intra-cluster distance as neighboring nodes are apt to be grouped in the same cluster for similarity of their embedding. Therefore, the intra-cluster distance can work to supervise when to stop the smoothing process in such a way that the smoothing will proceed if intra-cluster distance in current iteration is less than in the last and terminate otherwise. The following formula is used for calculating the intra-cluster distance [13]:

$$Intra(C) = \frac{1}{|C|} \sum_{k \in C} \frac{1}{|l|(|l|-1)} \sum_{\substack{v_i, v_j \in l, \\ v_i \neq v_j}} \|x_i' - x_j'\|^2 \quad (9)$$

$C$  is the set of cluster labels,  $|C|$  is the number of different cluster labels,  $v_i$  and  $v_j$  are different nodes assigned to the cluster label  $l$ ,  $|l|$  is the number of spots assigned to the cluster label  $l$ ,  $x_i'$  and  $x_j'$  are respectively the smoothed embeddings of  $v_i$  and  $v_j$ .

**Table 1**

Notation summary in STGIC.

Notation	Meaning
$\sigma$	Standard deviation of the Gaussian kernel function for computing Adjacency from distance matrix
$P_{adj}$	Pre-specified factor for searching for suitable $\sigma$
$Ncom_{precluster}$	Dimension number which is reduced to by PCA during input preparation for pre-clustering
$D_{kmeans}$	Dimensions which are reserved for Kmeans clustering during pre-clustering stage
$Ncom_{cluster}$	Dimension number which is reduced to by PCA during input preparation for clustering training rather than pre-clustering
$hvg_{num}$	Top number of highly variable genes selected to prepare input for clustering training rather than pre-clustering

---

$iter_{max}$	Maximum iteration number in pre-clustering
$X$	Feature matrix as input of pre-clustering
$X_{CNN}$	Feature matrix from which the input feature image for the CNN in STGIC is derived
$X_{img}$	Input feature image
$X'_{img}$	Perturbed input feature image
$A$	Adjacency
$L_s$	Symmetrically normalized Laplacian matrix
$\lambda_{max}$	Maximum eigen-value of $L_s$
$rate_{drop}$	Probability at which a channel of $X_{img}$ is masked with 0
$pretrain_{max}$	Pre-training iteration number
$train_{max}$	Training iteration number
$ratio_{K3}$	Weight of the feature image output by STGIC <sub>K3</sub>
$interval_{update}$	Update interval for the distribution $P$
$cut_{epoch}$	Epoch cutoff over which pseudo-label skill is used in training
$cut_q$	Clustering confidence cutoff
$ratio_{con}$	Weight of longitudinal and transverse smoothing loss
$ratio_{con1}$	Weight of diagonal smoothing loss
$ratio_{kl}$	Weight of KL divergence loss
$ratio_{gca}$	Weight of contrastive loss
$ratio_{ce}$	Weight of cross-entropy loss in training
$n_{clusters}$	Number of clusters
$tol$	Tolerance of the incidence by which the labels predicted by successive two iterations of the same spot are different
$E_{pixel}$	Weighted sum of outputs of the two frameworks STGIC <sub>K3</sub> and STGIC <sub>K4</sub> from the input $X_{img}$
$E'_{pixel}$	Weighted sum of outputs of the two frameworks STGIC <sub>K3</sub> and STGIC <sub>K4</sub> from the input $X'_{img}$
$M_{out}$	Embedding matrix extracted from $E_{pixel}$ according to lattice coordinates of all spot pixels
$M'_{out}$	Embedding matrix extracted from $E'_{pixel}$ according to lattice coordinates of all spot pixels
$Clu_{preclustering}$	Cluster partition generated by pre-clustering
$Clu_{pretraining}$	Cluster partition generated by pre-training
$Clu$	Final clustering result generated by trained STGIC
$\mu$	Trainable centroid matrix for training
$\tau$	Temperature factor for computing $L_{gca}$
$L_{gca}$	Contrastive loss as a component of the total loss for training
$L_{KL}$	KL divergence as a component of the total loss for training
$L_{pseudo}$	Cross-entropy computed with logits and pseudo-labels as a component of the total loss for training
$L_{transverse}$	Eucalidean distance between transversely neighboring spot pixels computed with their embedding
$L_{longitudinal}$	Eucalidean distance between longitudinally neighboring spot pixels computed with their embedding
$L_{diagonal}$	Eucalidean distance neighboring spot pixels along the main diagonal computed with their embedding
$L_{smooth}$	Weighted sum of $L_{transverse}$ , $L_{longitudinal}$ and $L_{diagonal}$

---

$L_{total}$	Total loss for training
$nChannel$	Output dim of the first three convolution layers of both the two frameworks $STGIC_{K3}$ and $STGIC_{K2}$
$D_{out}$	Output dim of the last convolution layers of both the two frameworks $STGIC_{K3}$ and $STGIC_{K2}$
$lr_{pretrain}$	Learning rate for pre-training
$lr$	Learning rate for training

### 3.3. Construction of STGIC

Our method STGIC combines AGC and dilated CNN-based framework together. The operation of STGIC can be divided into two stages, graph convolution-based pre-clustering and dilated CNN-based clustering. The clustering stage consists of two steps including pre-training and training. Pre-clustering stage use AGC to generate cluster labels as pseudo-labels for pre-training in the clustering stage. The pre-training step takes the above pseudo-labels and adopt cross-entropy as the loss function. Based on the values of the trainable parameters fixed by pre-training, the trainable centroid matrix for training stage is initiated. Besides, a trick for self-supervision through KL divergence, the method for forcing spatial continuity, another pseudo-label skill and contrastive learning are united to construct objective in the training step. In the following, the structural elements of STGIC is to be elucidated respectively. The notations thereof are listed in Table 1. The general structure of the dilated CNN-based frameworks in STGIC is presented in Fig. 2.

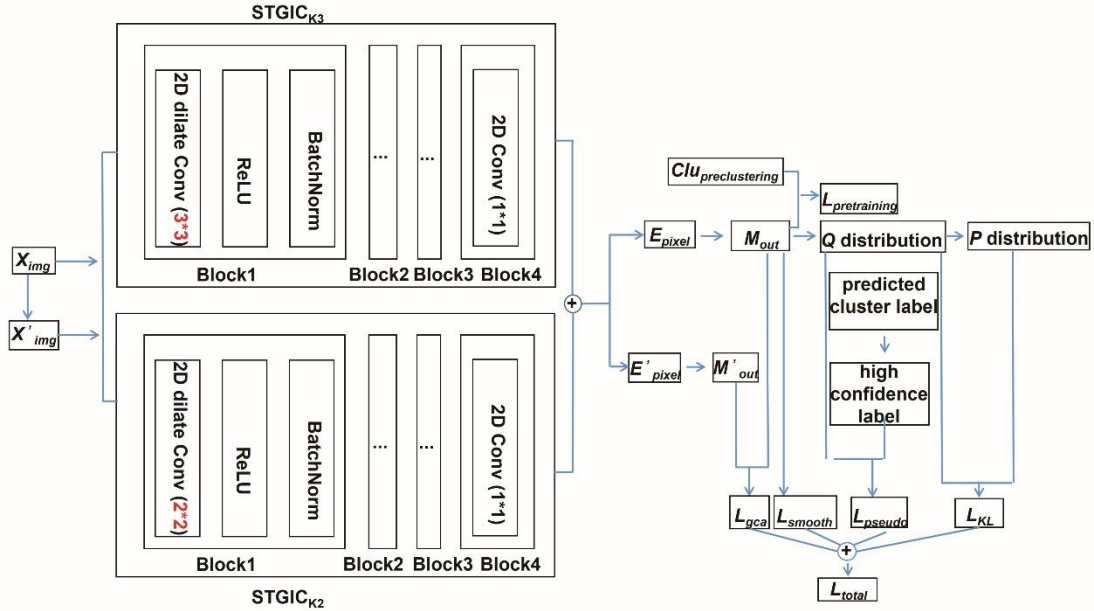


Fig. 2. General structure of the dilated CNN-based frameworks in STGIC.  $\oplus$  represents weighted sum.

#### 3.3.1. Pre-clustering with AGC in STGIC

Generally but not exactly, the transcription profile of each spot looks more like its

neighbor than that of spots spatially distant and spots in the same cluster in our problem are often grouped together spatially, hence the spatial distance between spots plays much more important role than in other common application field of GCN such as fMRI and EEG where functional correlation is the determinant, outshining the spatial distance. The adjacency herein is hence constructed with spatial distance. Instead of utilizing binary adjacency, we derive a distance matrix from pixel coordinates of each spot rather than lattice coordinates, since pixel coordinates reflect the practical spatial location. Following the practice of SpaGCN to generate the self-looped adjacency from distance matrix, we

derive the adjacency in the formula: 
$$A_{ij} = e^{-\frac{d_{ij}^2}{2\sigma^2}} \quad (10)[4]$$

$A_{ij}$  is the element of the adjacency  $A$  in row  $i$  and column  $j$ ,  $d_{ij}$  is the element of the distance matrix in row  $i$  and column  $j$ ,  $\sigma$  is a value which can make the mean of row sums of the difference matrix  $A-I$  equal a pre-specified hyper-parameter  $P_{adj}$ . The diagonal elements of the obtained adjacency matrix are all 1, since the distance between each spot and itself is always 0, hence the adjacency constructed in this way is self-looped.

The input features matrix  $X$  is prepared with the expression matrix. After filtering out repetitive genes and normalizing the expression matrix, Principal component analysis (PCA) is performed with the filtered and normalized expression matrix, the resulting matrix is of  $Ncom_{precluster}$  dimensions, the columns of which corresponds to all the remaining genes.

At the initial iteration, the  $t$  value in formula (8) is set to 1. the smoothed embedding multiplies with its own transpose generates a similarity matrix, the eigen-vector matrix of which can be used to carry out spectral clustering. The columns of the eigen-matrix are arranged such that the eigen-vector corresponding to larger eigen-value of has smaller column index. The top  $D_{kmeans}$  columns of the eigen-matrix is reserved. The above process is in fact a dimension reduction operation to generate the input for Kmeans, which realization of spectral clustering depends on. The dimension-reduced matrix is used to cluster with Kmeans, each spot is represented by the corresponding row vector. The cluster label assignment in this iteration is generated and then the intra-cluster distance is computed. Iteration will stop if the aforementioned termination condition of AGC is satisfied or reach the maximum iteration number  $iter_{max}$ . The structure of AGC in STGIC is illustrated in Fig. 3.

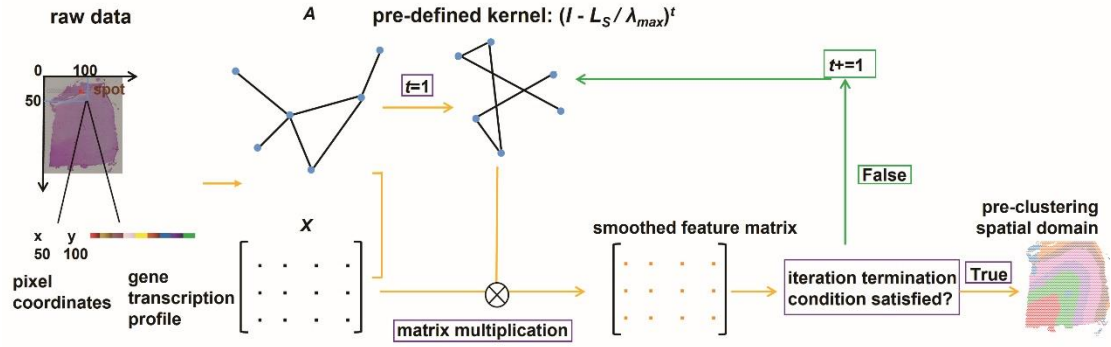


Fig. 3. Flowchart of STGIC pre-clustering with AGC.

### 3.3.2. CNN frameworks in STGIC

The pipeline for the generation of the feature matrix  $X_{CNN}$  for the CNN network in STGIC is different in some details from that for the preparation of pre-clustering input  $X$ . The PCA in this step is done with normalized transcription matrix of top  $hvg_{num}$  highly variable genes, rather than in the range of the whole filtered genes adopted in pre-clustering. Highly variable genes are selected by ascent ordering of the variance of gene transcription quantity among all spots. Besides, the dimension reduction parameter of  $Ncom_{cluster}$  doesn't have to be consistent with that for pre-clustering. Each row of the resulting PCA matrix corresponds to a spot, and a padding vector representing null pixels and background pixels is calculated by computing the top  $Ncom_{cluster}$  principal components of zero vector with the eigen-vectors generated in the PCA. After incorporating the padding vector into the PCA matrix as the last row, the normalization as to each column are done via division of the difference between each element and the minimum in the same column by that between the maximum and the minimum in the column so that all elements in the resulting normalized matrix are in the range of the interval  $[0, 1]$ , which is in accordance with that required by UISDC on input images.

The feature matrix  $X_{CNN}$  can be transformed into the input image  $X_{img}$  by arranging each spot at lattice coordinates rather than pixel coordinates. Pixels would be distributed too sparsely for the convolution kernel to gather surrounding information effectively if the pixel coordinates were adopted since a majority of pixels in the H&E staining image have no corresponding spots. At first, the maximum abscissa and ordinate are found out from lattice coordinates,  $X_{img}$  is generated with the Channel number equal to the column dimension of the above normalized matrix and the height and width of 1 larger than the maximum abscissa and ordinate since the coordinates start with 0 but not 1. Pixel values of all spot pixels adopt the values in the corresponding row of the above normalized matrix, those of all null pixels and background pixels adopt the values of the normalized padding vector in the last row of the normalized matrix. Noticeably, although null pixels and background pixels have identical pixel values, they should not be equated, since the background is thoroughly outside the spots area and no cells exists in background area

while null pixel is located in the spots area so that cells could have lied in the position corresponding to null pixel but the transcription information can't be gathered for technical limitations. Equating the two types of pixels may impact the performance of our method. However, the liability brought about by the identical padding can be circumvented by our adaptation of the original CNN framework in UISDC. We adopt the convolution kernel with dilate rate of 2 which ensures each spot pixel gathering information only from the neighboring spot pixels, successfully skipping null pixels. Another problem, nevertheless, may arise with the introduction of the dilation mechanism. If kernel size is set to 2, only 4 neighboring spot pixels of a spot pixel are framed in the kernel even excluding the spot pixel itself, whereas if kernel size is set to 3, the aforementioned 4 neighboring spots are omitted even though the spot pixel itself is included at the center. Among the other 8 spot pixels excluding the center, their distance from the center is larger than the 4 spot pixels framed in the kernel of size 2, especially, 4 spot pixels cornering the kernel of size 3 are so far from the center that inclusion of them for aggregation may decrease the performance in light of the dependence of correlation of spots on their spatial distance. This disadvantage can be overcome by the combination of kernels with size of both 2 and 3 and setting the kernel weight at the 4 corners of the latter to 0, whereby the updating of the feature of a spot pixel only depends on its top 8 neighboring spot pixels and itself as is done in the CNN of UISDC. To make sure aggregation by weights that are correlated with spatial distance, we set kernel weights to be identical at the position equally distant from the center. The receptive field of the dilated convolution kernel of size 2 and 3 and their aggregation manner are shown in Fig. 4. The adaptation of the CNN framework in UISDC establishes our own CNN frameworks in STGIC.

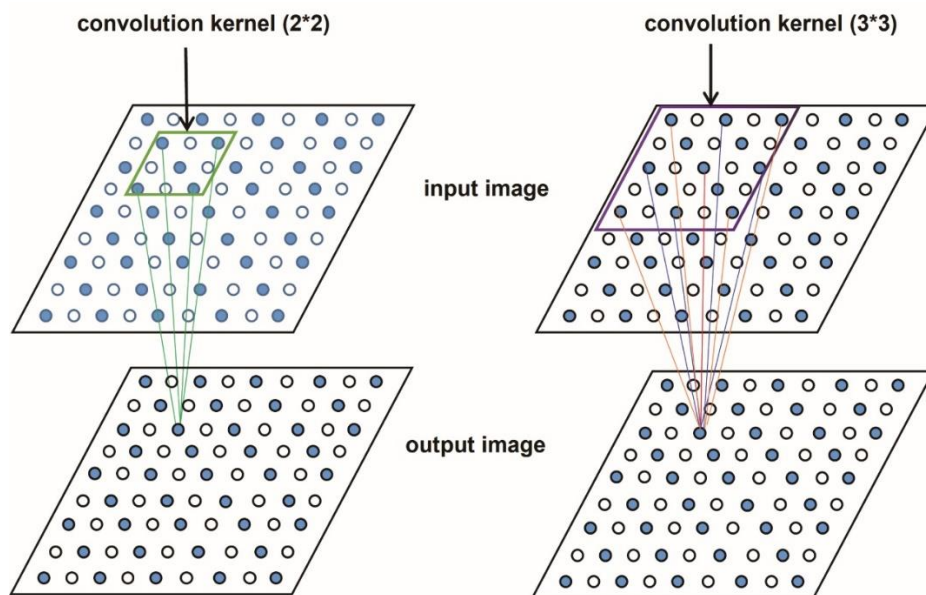


Fig. 4. Receptive field and the relationship between spatial position and weight values of the dilated CNN kernels of STGIC. Equal weight values corresponding to the position of the same distance from kernel center are represented with the same color. Weight values 0 of the kernel with size 3 are represented

with dark yellow to symbolize negligence of the spots at the four corners for aggregation.

To describe our CNN frameworks in detail. Two CNN frameworks  $STGIC_{K3}$  (corresponding to convolution kernel size 3) and  $STGIC_{K2}$  (corresponding to convolution kernel size 2) are employed in parallel. Each framework is composed of 4 convolution blocks. The first 3 blocks are composed sequentially of a dilated convolution layer, a batch normalization layer and a ReLU activation layer. The last block contains only a convolution layer with kernel size 1. The channel numbers of the first 3 blocks in both frameworks are set equal to  $nChannel$ , and those of the last blocks in them are all set to  $D_{out}$ . The difference of the two framework lies in the kernel size and padding size of the convolution layers in the first 3 blocks. The difference in kernel size of the first three layers of the two frameworks have been elucidated above. The padding size corresponding to kernel size 3 is 2 and that corresponding to kernel size 2 is 1 to keep the size of the output feature images always the same as  $X_{img}$ . Finally, outputs from the two frameworks is summed up by their respective weight,  $ratio_{K3}$  for  $STGIC_{K3}$  and  $1 - ratio_{K3}$  for the other. The weighted sum generates the final pixel embedding  $E_{pixel}$  in the form of a feature image with the number of channels equal to  $n_{clusters}$ .

### 3.3.3. Construction of objectives for pre-training of STGIC

As discussed above, the similarity in aggregation mode between GCN and the CNN of UISDC, together with the convertibility of the generated graph in ST data to image justifies the applicability of STGIC to the image derived from graph. In other words, the image output from our CNN frameworks,  $E_{pixel}$  may have some underlying characteristic in common with the output from GCN. Therefore,  $E_{pixel}$  may be amenable to the training objective originally designed for graph convolution. To preclude the interference from the null pixels, the embedding matrix  $M_{out}$  of spots pixels is extracted from  $E_{pixel}$  according to the lattice coordinates of each spot pixel and arranged according to spots indices adopted in the h5ad file.  $M_{out}$  can be used as a logits matrix for computing cross-entropy loss with pseudo labels generated by the pre-clustering result  $Clu_{preclustering}$ .

The pre-training adopts the cross-entropy as the loss function which is computed with the formula:

$$L_{pretraining} = -\sum_{s \in S} \sum_{l=1}^{|C_l|} c_{sl} \ln h_{sl} \quad (11)$$

$S$  is the set of spots in a sample,  $h_{sl}$  is the probability of spot  $s$  being assigned to the cluster label  $l$  and is an element in the spot  $s$  corresponding row of  $M_{out}$ ,  $c_{sl}$  equals 1 if spot  $s$  is assigned to the cluster label  $l$  by  $Clu_{preclustering}$  else 0.

After the completion of the pre-training, a cluster label assignment  $Clu_{pretraining}$  is generated by finding a column index for each row in which the maximum of a row appears in  $M_{out}$ .  $Clu_{pretraining}$  is used to initialize a trainable parameter matrix during training.



### 3.3.4. Construction of objectives for training of STGIC

The self-supervision loss as to GCN output designed by a deep graph clustering network algorithm SDCN [15] and also used by SpaGCN is adopted by us as a component of our loss function. But in STGIC, it is used to treat the CNN output  $M_{out}$ . It is fulfilled by the KL divergence loss between two distributions  $P$  and  $Q$ .  $Q$  is the probability distribution of each spot assigned to each cluster label which is computed with  $M_{out}$  and a trainable centroid matrix  $\mu$  of all clusters, each row of which corresponding to the centroid vector of one cluster.  $\mu$  is initialized with average of the row vectors of  $M_{out}$  corresponding to the same cluster according to  $Clu_{pretraining}$ . The distribution  $Q$  is computed with the

formula:

$$q_{ij} = \frac{(1 + \|h_i - \mu_j\|^2)^{-1}}{\sum_{j=1}^{|C|} (1 + \|h_i - \mu_j\|^2)^{-1}} \quad (12) [4]$$

$q_{ij}$  is the probability of spot  $i$  being assigned to the  $j^{th}$  cluster,  $h_i$  is the  $i^{th}$  row of  $M_{out}$ , namely the logits vector of spot  $i$ ,  $\mu_j$  is the  $j^{th}$  row of  $\mu$ , that is, the embedding vector of the centroid of the  $j^{th}$  cluster. The distribution  $P$  is calculated with  $Q$  in the formula:

$$p_{ij} = \frac{q_{ij}^2 / \sum_i q_{ij}}{\sum_j (q_{ij}^2 / \sum_i q_{ij})} \quad (13) [4]$$

The subscript  $i$  and  $j$  have the same meaning as those in  $q_{ij}$ . The KL divergence loss is

computed in the formula:

$$L_{KL} = \sum_i \sum_j p_{ij} \log \frac{p_{ij}}{q_{ij}} \quad (14) [4]$$

Unlike  $Q$  being updated each iteration,  $P$  is only updated every  $interval_{update}$  iterations. At the end of every iteration, a clustering label assignment is obtained by finding in the  $Q$  distribution the column index at which the element value is the largest as to each row, reflecting the most likely cluster each spot belonging to.

The smoothing related loss is inherited from UISDC to ensure spatial continuity among embedding of spot pixels, but is adapted to our own needs. In fact, the term ‘spatial continuity’ in UISDC have the same meaning with the word ‘smoothness’ as to graph convolution method. CNN operation seems to be not so capable of conducting to embedding smoothness as graph convolution, hence the eucalidean distances between neighboring pixels is computed as a part of loss to force smoothness in UISDC. Here, we force the smoothness of spot pixels in three directions. Besides distances of all pairs of longitudinal and transverse neighboring spot pixels separated by one null pixel, those of pairs of neighboring spot pixels in the direction of  $45^\circ$  (described as in the diagonal direction for brevity) are also computed. The longitudinal loss  $L_{longitudinal}$  and the transverse loss  $L_{transverse}$  are both weighted by  $ratio_{con}$  while the diagonal loss  $L_{diagonal}$  is weighted by  $ratio_{con1}$ , since the 2D spatial distances of the nearest spot pixels in longitudinal and

transverse are equal while don't tally with that in diagonal. The loss to force spatial continuity is computed in the formula:

$$L_{smooth} = ratio_{con} * (L_{longitudinal} + L_{transverse}) + ratio_{con1} * L_{diagonal} \quad (15)$$

Pseudo-labels are also used during training after the first  $cut_{epoch}$  iterations. The pseudo-labels here is not the pre-clustering generated labels during pre-training iteration but derived from the Q distribution in current iteration of our training stage. As has been described, a cluster label assignment is generated in every training iteration and the corresponding elements in the Q distribution matrix present the confidence for each cluster label. The labels with the confidence higher than  $cut_q$  are taken as pseudo-labels. The classic cross-entropy loss, denoted as  $L_{pseudo}$ , between the pseudo-labels and the corresponding embedding extracted from  $M_{out}$  are computed as in the pre-training loss.

The contrastive loss is constructed following GCA [16]. GCA adopts a contrastive learning skill in graph learning. The original graph is set as view 1 and the graph perturbed on the feature input by substituting some randomly chosen columns with 0 is set as view 2. The embedding of the same node from both views constitutes a positive pair, that of one node from view 1 and that of other nodes from view2 constitutes inter-view negative pairs, that of one node from view1 and other nodes also from view1 constitutes intra-view negative pairs. Embedding similarities within each pair are computed followed by softmax and logarithm to estimate the relative similarity of each node from the two views in the

following formula:

$$\ell(u_i, v_i) = \log \frac{e^{\theta(u_i, v_i)/\tau}}{e^{\theta(u_i, v_i)/\tau} + \sum_{n \neq i} e^{\theta(u_i, v_n)/\tau} + \sum_{n \neq i} e^{\theta(u_i, u_n)/\tau}} \quad (16)$$

$u_i$  and  $v_i$  denotes embedding of the  $i^{th}$  node from view 1 and view 2,  $\theta$  is cosine similarity function and  $\tau$  is a temperature factor. The loss function of GCA based on the relative similarity is computed in the formula:

$$L_{gca} = -\frac{1}{2N} \sum_{i=1}^N (\ell(u_i, v_i) + \ell(v_i, u_i)) \quad (17)$$

N is the total number of nodes in a graph. In our scenario, the probability at which one channel of the input image  $X_{img}$  is to be masked with 0 is controlled by  $rate_{drop}$  and the perturbation generates an input image  $X'_{img}$ .  $M_{out}$ , spots embedding from view 1 and its counterpart  $M'_{out}$  from  $X'_{img}$  are used to compute the cosine similarity between spots. The contrastive loss  $L_{gca}$  is computed in the formula (16) and (17).

The final loss function in our training stage can be expressed as

$$L_{total} = ratio_{kl} * L_{KL} + L_{smooth} + ratio_{ce} * L_{pseudo} + ratio_{gca} * L_{gca} \quad (18)$$

The training iteration will terminate if the number of unique predicted cluster labels is less than that specified by the ground-truth or the percentage of spots having a predicted label different from that predicted in the last iteration is less than  $tol$ .

## 4. Experimental results

We evaluate the clustering performance of our STGIC with all the 12 samples in the dataset DLPFC and compare with SpaGCN, BayesSpace, STAGATE and SpatialPCA.

### 4.1. Datasets specification

The 12 samples of DLPFC can be divided into 3 groups by the shape of ground-truth specified spatial domains, each group containing 4 samples. The samples with sample id from 151507 to 151510 all consist of 7 clusters and nearly all the spatial domains look like straight strip, those with id from 151669 to 151672 all consist of 5 clusters and all the spatial domains present single gentle wave shape, those with id from 151673 to 151676 all comprise 7 clusters and all the spatial domains present obvious arcs.

### 4.2. Baselines and evaluation metrics

Four methods are used as baseline. Among them, two are based on graph learning, including SpaGCN and STAGATE, while the other two are statistical models including BayesSpace and SpatialPCA. Following the convention of performance test of ST clustering algorithm, STGIC is tested with identical hyper-parameters among all the 12 samples for each algorithm. Comparison in performance can be made between STGIC and the baseline by Adjusted Rand Index (ARI) computed with the predicted clustering labels and the ground-truth. The higher ARI means a better performance. Both the mean and median ARI among the 12 samples are computed to indicate the general performance.

### 4.3. Parameter settings

Although  $\lambda_{max}$  is approximated to be 2 in AGC, we follow the practice of AGE [17] by setting it to be 1.5 since the average of maximum eigen-values of Laplacian matrices of the 12 samples is closer to 1.5 than 2, hence we set  $\lambda_{max}$  to be 1.5 for all the samples. random seeds of the python package numpy, pytorch and random are all set to 0. The hyper-parameter of random state for Kmeans by Scikit-learn in each iteration during pre-clustering is set to be 0, 42 and 20. Adam optimizer is used for both pre-training and training. The hyper-parameter  $n_{clusters}$  is set according to the number of unique cluster labels in the ground truth. All the hyper-parameters setting is recorded in Table 2.

**Table 2**

Parameter settings of STGIC

Notation	Value
$\lambda_{max}$	1.5
$P_{adj}$	0.5
$N_{com_{precluster}}$	50
$D_{kmeans}$	26

$N_{com_{cluster}}$	15
$ratio_{K3}$	0.7
$hvg_{num}$	3000
nChannel	100
$D_{out}$	100
$\tau$	0.3
$ratio_{con}$	0.62
$ratio_{con1}$	0.63
$ratio_{kl}$	0.95
$ratio_{gca}$	0.025
$ratio_{ce}$	0.53
$rate_{drop}$	0.33
$tol$	0.001
$cut_q$	0.5
$interval_{update}$	4
$cut_{epoch}$	4
$iter_{max}$	30
$pretrain_{max}$	200
$train_{max}$	400
$lr_{pretrain}$	0.05
$lr$	0.02

#### 4.4. Software and Package Version

To facilitate the reproduction of our results, the versions of all software and packages in our research is presented in Table 3.

**Table 3**

Version of software and packages in our research.

Package	Version
Python	3.8.13
torchvision	0.8.2
Pytorch	1.13.0+cu117
numpy	1.20.1
pandas	1.2.1
scikit-learn	0.23.2
scanpy	1.9.1
opencv-python	4.6.0.66
skmisc	0.1.4
scipy	1.6.2

#### 4.5. Performance comparison

Our pre-clustering attains better performance than all the baseline methods, judged by both the mean and median ARI among all the tested samples, except for a little

disadvantage in the median ARI 0.536 compared with 0.542, that of SpatialPCA. The training of the dilated-CNN network in STGIC raises ARIs of a majority of samples except for 151671, 151672 and 151675 in which the drop is no more than 0.013. It is noteworthy that STGIC perform well on 151669 and 151670 which are setbacks nearly all the graph-based methods are confronted with. Ultimately, STGIC outperforms all the baseline significantly in terms of the mean and median ARI. ARIs are all listed in Table 4 except for those of SpatialPCA since the paper reporting SpatialPCA only provides the median ARI of 0.542 without the value of each sample [7].

**Table 4**

Clustering performance.  $STGIC_{pre}$  means ARI computed with the result of pre-clustering of our STGIC,  $STGIC_{train}$  means ARI computed with the final result of our trained STGIC deep network. ARIs of each sample with STAGATE and BayesSpace are all cited from the supplementary information of the paper reporting STAGATE [5]. The performance of SpaGCN is cited from the paper reporting SpaGCN [4]. The mean and median ARIs attained by our trained STGIC model are highlighted in blue.

ID <sub>sample</sub>	STGIC <sub>pre</sub>	STGIC <sub>train</sub>	SpaGCN	STAGATE	BayesSpace
151507	0.506	0.554	0.488	0.530	0.460
151508	0.411	0.423	0.432	0.510	0.420
151509	0.495	0.598	0.441	0.470	0.480
151510	0.450	0.635	0.449	0.460	0.450
151669	0.426	0.685	0.245	0.330	0.470
151670	0.386	0.519	0.369	0.310	0.300
151671	0.565	0.563	0.517	0.500	0.500
151672	0.576	0.563	0.572	0.540	0.770
151673	0.617	0.649	0.525	0.580	0.550
151674	0.644	0.652	0.389	0.610	0.440
151675	0.603	0.594	0.461	0.620	0.530
151676	0.595	0.611	0.348	0.600	0.440
mean	0.523	0.587	0.436	0.505	0.484
median	0.536	0.596	0.445	0.520	0.465

#### 4.6 Ablation study

As shown in the formula (18), the loss function for training of our methods is composed of four components:  $L_{KL}$ ,  $L_{smooth}$ ,  $L_{gca}$  and  $L_{pseudo}$ . To clarify the contribution made by each part to clustering performance. The ablation study begins with the loss function only reserving  $L_{KL}$ , and then involves the other components in turn except the last one since the performance with the integral loss function has been shown in Table 4. When one component is incorporated in the loss function, the corresponding weight keep the same as that in the formula (18).

Self-supervision alone via KL divergence doesn't nearly make any difference,

compared with the pre-clustering performance. The involvement of the second component to force embedding similarities between neighboring spot pixel significantly improves the performance. Subsequent addition of pseudo-labels related cross-entropy loss lifts the performance if judged by the mean ARI, yet causes a little drop to the median. Comparing the performance in this step with our final performance highlighted in blue in Table 4, we find that the contrastive learning also rises the performance by a very limited extent.

**Table 5**

Ablation study. Among the four components of loss function in formula (18), Component1 contains only the first one, Component12 contains the first two components and Component123 contains the first three components.

ID <sub>sample</sub>	Component1	Component12	Component123
151507	0.529	0.553	0.552
151508	0.416	0.421	0.410
151509	0.511	0.518	0.563
151510	0.436	0.485	0.626
151669	0.399	0.615	0.702
151670	0.365	0.438	0.521
151671	0.549	0.595	0.557
151672	0.585	0.566	0.566
151673	0.608	0.664	0.643
151674	0.648	0.682	0.664
151675	0.598	0.612	0.593
151676	0.579	0.608	0.610
mean	0.519	0.563	0.584
median	0.539	0.581	0.580

---

### Algorithm 1 STGIC

---

**Input:** pixel coordinates, lattice coordinates,  $X$ ,  $\lambda_{max}$ ,  $X_{img}$ ,  $rate_{drop}$ ,  $pretrain_{max}$ ,  $train_{max}$ ,  $ratio_{K3}$ ,  $interval_{update}$ ,  $cut_{epoch}$ ,  $cut_q$ ,  $ratio_{con}$ ,  $ratio_{con1}$ ,  $ratio_{kl}$ ,  $ratio_{gca}$ ,  $ratio_{ce}$ ,  $n_{clusters}$ ,  $tol$

**Output:** Cluster partition  $Clu$

- 1: Compute adjacency  $A$  with pixel coordinates
  - 2: Transform  $X$  into input image  $X_{img}$  according to lattice coordinates
  - 3: Pre-clustering via AGC with  $A$ ,  $X$  and  $\lambda_{max}$  to generate a label assignment for pre-training pseudo-labels  $Clu_{preclustering}$ .
  - 4: for iter in range( $pretrain_{max}$ ):
  - 5:  $E_{pixel} = ratio_{K3} * STGIC_{K3}(X_{img}) + (1 - ratio_{K3}) * STGIC_{K2}(X_{img})$
  - 6: Obtain  $M_{out}$  from  $E_{pixel}$  according to the lattice coordinates of all spot pixels
  - 7: Compute  $L_{pretraining}$  from  $Clu_{preclustering}$  and  $M_{out}$  with formula (11)
  - 8: Optimize  $L_{pretraining}$  and update the trainable parameters
-

---

9:  $\text{Pred}_{\text{last}} = \text{argmax}(M_{\text{out}}, 1)$

10: Derive the cluster label assignment  $\text{Clu}_{\text{pretraining}}$  generated by pre-training with  $\text{argmax}(E_{\text{pixel}}, \text{axis} = 1)$

11: Initialize the trainable centroid matrix  $\mu$  with  $M_{\text{out}}$  and  $\text{Clu}_{\text{pretraining}}$  by grouping the spots with the same label and compute the average embedding

12: for iter in range( $\text{train}_{\text{max}}$ ):

13: Perturb  $X_{\text{img}}$  with the probability  $\text{rate}_{\text{drop}}$  to get the perturbed input image  $X'_{\text{img}}$

14:  $E_{\text{pixel}} = \text{ratio}_{\text{K3}} * \text{STGIC}_{\text{K3}}(X_{\text{img}}) + (1 - \text{ratio}_{\text{K3}}) * \text{STGIC}_{\text{K2}}(X_{\text{img}})$

15:  $E'_{\text{pixel}} = \text{ratio}_{\text{K3}} * \text{STGIC}_{\text{K3}}(X'_{\text{img}}) + (1 - \text{ratio}_{\text{K3}}) * \text{STGIC}_{\text{K2}}(X'_{\text{img}})$

16: Obtain  $M_{\text{out}}$  from  $E_{\text{pixel}}$  according to the lattice coordinates of all spot pixels

17: Obtain  $M'_{\text{out}}$  from  $E'_{\text{pixel}}$  according to the lattice coordinates of all spot pixels

18: Compute the distribution Q from  $\mu$  and  $M_{\text{out}}$  with formula (12)

19:  $\text{Pred} = \text{argmax}(Q, \text{axis} = 1)$

20: if iter %  $\text{interval}_{\text{update}} == 0$ :

21: Compute the distribution P from Q with formula (13)

22: Compute  $L_{\text{KL}}$  from P and Q with formula (14)

23: Compute  $L_{\text{smooth}}$  which is the distance between neighboring spot pixels with the embedding from  $M_{\text{out}}$  with formula (15)

24: Compute the contrastive loss  $L_{\text{gca}}$  from  $E_{\text{pixel}}$  and  $E'_{\text{pixel}}$  with formula (16) and (17)

25: if iter >=  $\text{cut}_{\text{epoch}}$ :

26: Compute clustering confidence with  $\text{argmax}(Q, \text{axis}=1)$

27: Derive pseudo-labels from those spots whose clustering confidence is higher than  $\text{cut}_q$

28: Compute the cross-entropy as  $L_{\text{pseudo}}$  from the pseudo-labels and  $M_{\text{out}}$

29: Compute the total loss  $L_{\text{total}}$  with formula (18)

30: else:

31: Compute the total loss  $L_{\text{total}}$  with formula (18) but excluding the term of  $L_{\text{pseudo}}$

32: Optimize  $L_{\text{total}}$  and update the trainable parameters

33: Compute  $\text{delta}_{\text{label}}$  which is the percentage of different element between Pred and  $\text{Pred}_{\text{last}}$

34: if the number of the unique labels contained in Pred equals  $n_{\text{clusters}}$ :

35:  $\text{Pred}_{\text{last}} = \text{Pred}$

36: if iter > 0 and (iter-1) %  $\text{interval}_{\text{update}} == 0$  and  $\text{delta}_{\text{label}} < \text{tol}$ :

37: break

38: else:

39: break

40: Adopt  $\text{Pred}_{\text{last}}$  as the final clustering result  $\text{Clu}$

---

#### 4.7. Visualization

To intuitively show the performance of STGIC on the 12 samples from DLPFC, the spatial domains identified by our pre-clustering and clustering are presented together with the ground-truth as a reference. The ground-truth label '-1' means the cluster label is missing in the ground truth, as mentioned, the spots with no ground truth label are miniscule. STGIC<sub>pre</sub> presents the spatial domains generated by our pre-clustering and STGIC<sub>train</sub> presents the spatial domains generated by our ultimate clustering results. The unique label numbers of our pre-clustering and final results are all consistent with those of ground-truth, although the spots corresponding to some labels in our results seem to be invisible for their inappreciable quantity. Besides, it is also noteworthy that the visualization of our results doesn't adopt the same color-label mapping as the ground-truth. The visualization is presented in Fig. 5.



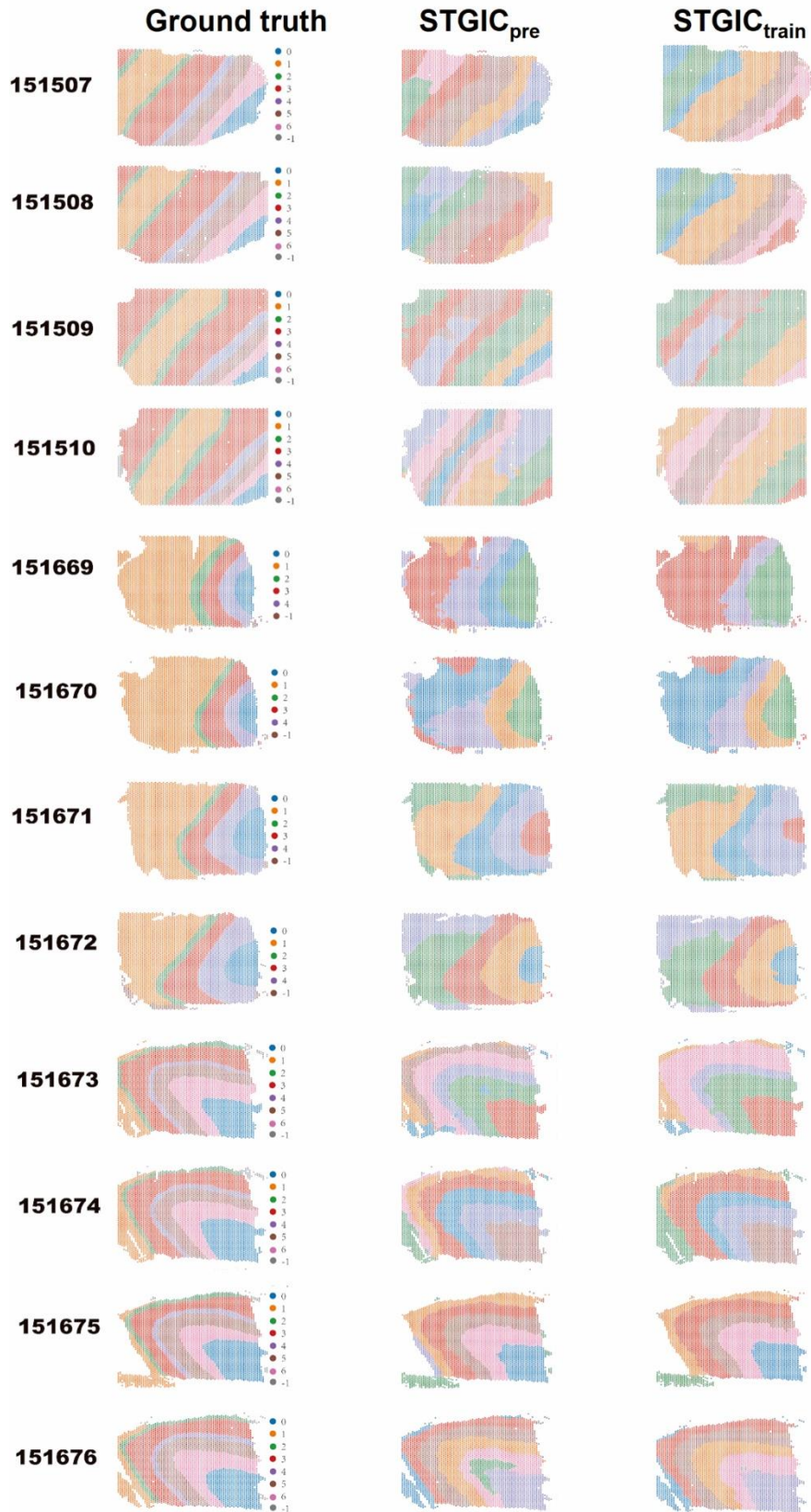


Fig. 5. Visualization of spatial domains of the 12 samples from DLPFC. The column names have the same meaning as that in Table 4. The color legend is only for ground truth and have nothing to do with STGIC<sub>pre</sub> and STGIC<sub>train</sub>.

## 5. Discussion

The collection of the 12 samples from DLPFC have been become the benchmark set for testing performance of ST clustering for their highly recognizable ground truth. ARI is a preferable index to estimate the performance compared with NMI for the problem and so the comparison in performance of different ST clustering methods often depend only on ARI. This practice is reasonable since ARI and NMI are positively correlated and ARI is significantly lower than NMI for the same sample analyzed with the same algorithm. The samples can be divided into three groups, as we have described. Each existing method tends to perform unequally among the three groups, namely, a method may have very low ARI on a majority of samples while an extraordinarily high ARI on one sample. The only singularly high value may likely raise the average, leading to an over-estimation of performance which can be avoid by computing median ARI instead of mean. That's why most papers thereof compute the median ARI for comparison. Here we compute both median and mean, median is the main index to reflect the general performance and simultaneously mean can also be referred to as a secondary index.

Our pre-clustering method performs no worse than many baseline methods, though the mean and median ARI is severely impacted by the poor performance on the samples of 151669 and 151670. However, it is noted that the bad performance on the two samples is not peculiar to our pre-clustering method AGC, as the baseline methods also perform much worse on them compared with on other samples. The visualization of the two samples shows the ground truth cluster label '1' is assigned to a majority of spots and corresponds to the spatial domain in orange while the counterparts of the domain according to our pre-clustering results are mainly split into two domains of about equal size and one domain of much smaller size, which suggests under-smoothing may occur to lead the single orange domain to be divided in the pre-clustering visualization for low similarity of spots embedding among the three domains constitutes the counterpart. This division is lessened in our final clustering result since the counterpart area is dominated by single domain with other two domains being significantly smaller, which suggests a better smoothness in the counterpart areas is achieved after training our network so that a single domain gathering a majority of spots in the counterpart area with similar embedding dominates. The rise of the ARIs of the two samples is possibly caused by the improvement of smoothing, as coincides with what is demonstrated by the ablation study in which the training objective about spatial continuity adapted from UISDC improves the performance significantly.

The final clustering result of STGIC performs much better than all baseline methods, although the visualization shows a seemingly lacking of one type of cluster label in our final results in several samples which in fact has the same number of unique cluster labels as that of ground truth since the training iteration will terminate once the number of the

unique labels predicted in current iteration is less than  $n_{clusters}$  which is specified by the unique labels number of ground truth and the predicted result of the last iteration is taken as the final result. The superiority of our method is demonstrated by the median and mean ARI. In addition, only the sample 151508 have a low ARI value below 0.45 while the other methods always generate low ARI on more than one sample which are even below 0.35. The comparison in this aspect indicate a relatively stable performance among all the testing samples.

## 6. Conclusion

We propose a graph convolution and image convolution combinatorial method STGIC to solve ST clustering problem. The graph convolution framework with predefined kernel is used for pre-clustering which provides pseudo-labels of high quality for pre-training of the two parallel-operating dilated CNN frameworks with different kernel sizes. The resulting embedding are subject to the supervision from pre-clustering labels with cross-entropy loss function for pre-training. During training, the embedding is treated with 4 training objectives. The first is KL divergence between the cluster assignment probability distribution and its derivative, the second is constraints on embedding dissimilarity between spatially neighboring spots, the third is cross-entropy between predicted cluster labels of high confidence and corresponding spots embedding and the last is contrastive loss from comparison between the above embedding and another generated from randomly perturbed input. The fancied framework is tested on the publicly recognized dataset DLPFC with 12 samples, outperforming the state-of-the-art methods in terms of mean ARI, median ARI and stability.

## CRedit authorship contribution statement

Chen Zhang: Conceptualization, Methodology, Writing - original draft. Junhui Gao: Conceptualization, Validation, Writing - review. Guangshuo Cao: Data preprocessing, Writing - editing. Wei Liu: Data preprocessing, Visualization.

## Declaration of competing interest

The authors declare that they have no known competing financial interests or personal relationships that could have appeared to influence the work reported in this paper.

## References

- [1] V.A. Traag, L. Waltman, N.J. van Eck, From Louvain to Leiden: guaranteeing well-connected communities, *Sci Rep.* 9 (2019). <https://doi.org/10.1038/s41598-019-41695-z>.

- [2] R. Dries, J. Chen, N. Del Rossi, M.M. Khan, A. Sistig, G.C. Yuan, Advances in spatial transcriptomic data analysis, *Genome Res.* 31 (2021) 1706–1718. <https://doi.org/10.1101/gr.275224.121>.
- [3] K.R. Maynard, L. Collado-Torres, L.M. Weber, C. Uytingco, B.K. Barry, S.R. Williams, J.L. Catallini, M.N. Tran, Z. Besich, M. Tippani, J. Chew, Y. Yin, J.E. Kleinman, T.M. Hyde, N. Rao, S.C. Hicks, K. Martinowich, A.E. Jaffe, Transcriptome-scale spatial gene expression in the human dorsolateral prefrontal cortex, *Nat Neurosci.* 24 (2021) 425–436. <https://doi.org/10.1038/s41593-020-00787-0>.
- [4] J. Hu, X. Li, K. Coleman, A. Schroeder, N. Ma, D.J. Irwin, E.B. Lee, R.T. Shinohara, M. Li, SpaGCN: Integrating gene expression, spatial location and histology to identify spatial domains and spatially variable genes by graph convolutional network, *Nat Methods.* 18 (2021) 1342–1351. <https://doi.org/10.1038/s41592-021-01255-8>.
- [5] K. Dong, S. Zhang, Deciphering spatial domains from spatially resolved transcriptomics with an adaptive graph attention auto-encoder, *Nat Commun.* 13 (2022). <https://doi.org/10.1038/s41467-022-29439-6>.
- [6] E. Zhao, M.R. Stone, X. Ren, J. Guenthoer, K.S. Smythe, T. Pulliam, S.R. Williams, C.R. Uytingco, S.E.B. Taylor, P. Nghiem, J.H. Bielas, R. Gottardo, Spatial transcriptomics at subspot resolution with BayesSpace, *Nat Biotechnol.* 39 (2021) 1375–1384. <https://doi.org/10.1038/s41587-021-00935-2>.
- [7] L. Shang, X. Zhou, Spatially aware dimension reduction for spatial transcriptomics, *Nat Commun.* 13 (2022). <https://doi.org/10.1038/s41467-022-34879-1>.
- [8] T.N. Kipf, M. Welling, Semi-Supervised Classification with Graph Convolutional Networks, (2016). <http://arxiv.org/abs/1609.02907>.
- [9] W. Kim, A. Kanezaki, M. Tanaka, Unsupervised Learning of Image Segmentation Based on Differentiable Feature Clustering, (2020). <https://doi.org/10.1109/TIP.2020.3011269>.
- [10] P. Veličković, W. Fedus, W.L. Hamilton, P. Liò, Y. Bengio, R.D. Hjelm, Deep Graph Infomax, (2018). <http://arxiv.org/abs/1809.10341>.
- [11] C. Mavromatis, G. Karypis, Graph InfoClust: Leveraging cluster-level node information for unsupervised graph representation learning, (2020). <http://arxiv.org/abs/2009.06946>.
- [12] Y. Liu, W. Tu, S. Zhou, X. Liu, L. Song, X. Yang, E. Zhu, Deep Graph Clustering via Dual Correlation Reduction, (2021). <http://arxiv.org/abs/2112.14772>.
- [13] X. Zhang, H. Liu, Q. Li, X.-M. Wu, Attributed Graph Clustering via Adaptive Graph Convolution, (2019). <http://arxiv.org/abs/1906.01210>.
- [14] F.A. Wolf, P. Angerer, F.J. Theis, SCANPY: Large-scale single-cell gene expression

- data analysis, *Genome Biol.* 19 (2018). <https://doi.org/10.1186/s13059-017-1382-0>.
- [15] D. Bo, X. Wang, C. Shi, M. Zhu, E. Lu, P. Cui, Structural Deep Clustering Network, in: *The Web Conference 2020 - Proceedings of the World Wide Web Conference, WWW 2020*, Association for Computing Machinery, Inc, 2020: pp. 1400–1410. <https://doi.org/10.1145/3366423.3380214>.
- [16] Y. Zhu, Y. Xu, F. Yu, Q. Liu, S. Wu, L. Wang, Graph contrastive learning with adaptive augmentation, in: *The Web Conference 2021 - Proceedings of the World Wide Web Conference, WWW 2021*, Association for Computing Machinery, Inc, 2021: pp. 2069–2080. <https://doi.org/10.1145/3442381.3449802>.
- [17] G. Cui, J. Zhou, C. Yang, Z. Liu, Adaptive Graph Encoder for Attributed Graph Embedding, in: *Proceedings of the ACM SIGKDD International Conference on Knowledge Discovery and Data Mining*, Association for Computing Machinery, 2020: pp. 976–985. <https://doi.org/10.1145/3394486.3403140>.